Friction of Shear-Fracture Zones

T. I. Riikilä,[1,2] J. I. Pylväinen,[1] and J. Åström[3]
[1]Department of Physics and Nanoscience Center, University of Jyväskylä, P.O. Box 35 (YFL), FI-40014 Jyväskylä, Finland
[2]Arctic Center, Lapland University, 96101 Rovaniemi, Finland
[3]CSC—It-center for science, P.O.Box 405, FIN-02101 Esbo, Finland
(Received 26 June 2017; published 20 December 2017)

A shear fracture of brittle solids under compression undergoes a substantial evolution from the initial microcracking to a fully formed powder-filled shear zone. Experiments covering the entire process are relatively easy to conduct, but they are very difficult to investigate in detail. Numerically, the large strain limit has remained a challenge. An efficient simulation model and a custom-made experimental device are employed to test to what extent a shear fracture alone is sufficient to drive material to spontaneous self-lubrication. A "weak shear zone" is an important concept in geology, and a large number of explanations, specific for tectonic conditions, have been proposed. We demonstrate here that weak shear zones are far more general, and that their emergence only demands that a microscopic, i.e., fragment-scale, stress relaxation mechanism develops during the fracture process.

DOI: 10.1103/PhysRevLett.119.255501

Fragmentation and fracture of materials is a class of fundamental material-physics processes that still have inadequate aspects of established theory. The formation of single cracks and tensile fragmentation, which is the result of many interacting single cracks, are reasonably well understood. The most difficult type of material fracture, fully developed compressive shear fragmentation at large strains, is also perhaps the most important. This type of fracture includes, apart from the initial crack propagation and the formation of a crack network and fragments, a grinding phase in which the early fragments are slowly ground to a powder.

Fracture in shear zones has been the subject of a large number of experimental [1–3] and numerical investigations [4–11]. These investigations are typically focused on small strains and the effective friction that appears near the early peak in shear stress or shortly thereafter. If the objective is to evaluate the shear strength of, e.g., a rock joint, this approach is appropriate, but it gives little or no information of the large-strain mechanical behavior. Reported results in the large-strain limit are also inconsistent. For example, in [3], higher confining pressure did not have an effect to friction coefficient, whereas in [2], higher confining pressure reduced friction.

Some of the most important applications of shear fracture can be found within the fields of geophysics and mining technology. The grinding of minerals to powder—comminution—in order to extract metals from minerals, consumes a significant fraction of the global yearly energy production, and any optimization of this is of huge economical and environmental significance [12,13]. In geophysics, the triggering failure in landslides and snow avalanches are typically shear fractures, and perhaps the most magnificent fractured shear zones of all are tectonic faults. Some of these faults have a surprisingly low effective friction (0.1) [14]. There are many suggested explanations for this, of which most refer to specific tectonic conditions [15], or mineral or gouge geology [16]. An exception would be, e.g., statically strong but dynamically weak faults [17,18]. From a physics point of view, a relevant question is whether weak shear zones are specific to tectonic environments, or if they appear under more general conditions.

In order to test if spontaneous self-lubrication, induced by fragmentation, is a generic phenomenon, we constructed a minimalistic, scale-invariant, computationally efficient numerical model. The model must be minimalistic in the sense that it contains only the essential physics with no reference to any specific material or environment. Scale invariance means that the model length scale needs to be rescalable to prove that observed phenomena may appear at many length scales. The numerical model must be computationally efficient to collect enough statistics, and the results are finally compared to experiments and observations.

The numerical model [19,20] material used here is constructed by numerically sedimenting two-dimensional, random-sized inelastic discs, which are fused together by massless inelastic beams. Discs in contact also interact via kinetic friction. Material samples in rectangular shear cells with periodic boundary conditions in the shear direction are broken by a forced shear strain. The beams stretch, bend, and break if deformed beyond a fracture threshold in elastic energy. The numerical algorithm is described in detail in Ref. [19]. To model the large strain limit, strains of up to 200% were simulated using $\sim 10^7$ time steps in each of the hundreds of simulations containing $\sim 10^4$ discs (Fig. 1).

Experiments on granite were performed with equipment designed exclusively for this purpose. The design is

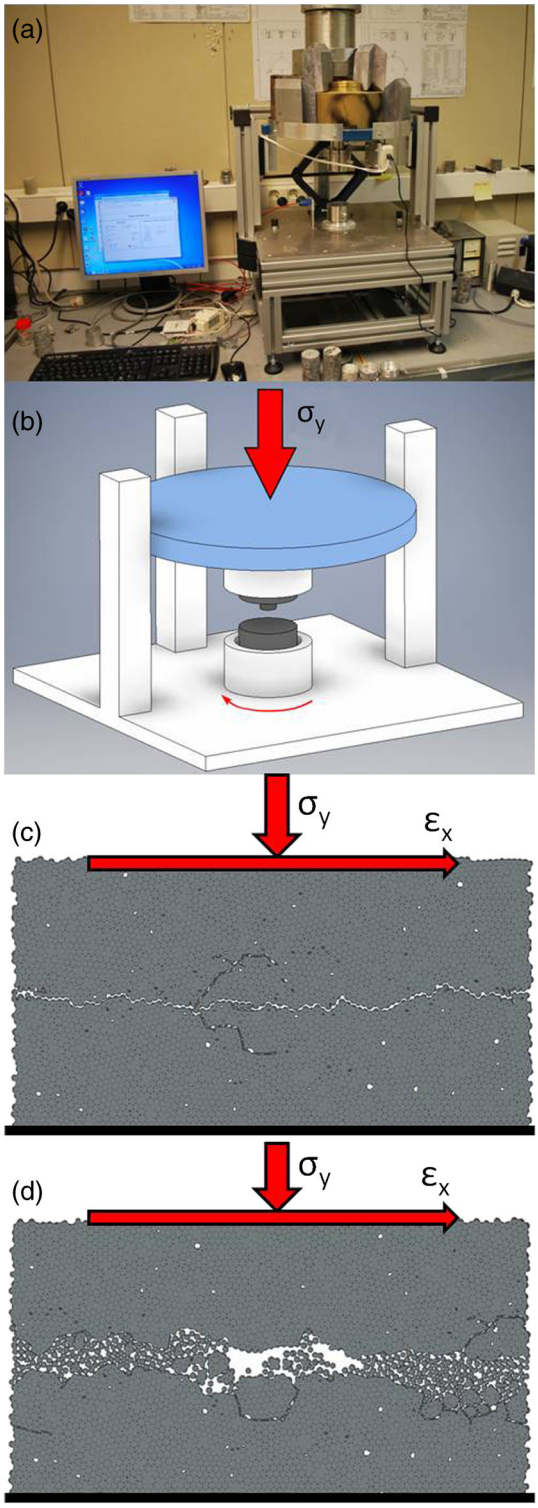

FIG. 1. The experimental equipment is shown in (a) together with a schematic presentation of the machine (b). In (c) the simulation setup is shown with the initial crack and in (d) after shearing.

displayed in Fig. 1, together with a schematic illustration of its working principle. Four different types of granite drill cores from the Olkiluoto region in Western Finland were used. They were prepared by making a shallow circular cut around the cylindrical surface of the drill core, and then breaking the sample in half with a hammer. This produced a natural crack surface. The grinding of the shear zone was then done by twisting the lower half while the upper half was pressed against it. Very large strains could be obtained in this way. The only stopping criteria used was attainment of reasonably constant sliding friction.

As mentioned above, shear-zone formation typically begins with small cracks that grow and coalesce to form a crack network and initial fragments. As shear strain increases, more cracks are formed and the initial fragments break up into smaller pieces that eventually turn into a fine powder. This process is composed of a large number, n_b, of localized fracture events. To construct a theory for effective macroscopic friction, μ_M, we need to define a few parameters. The tangential shear stress is τ_x, and the compressive stress across the shear zone is σ_y. Effective friction is then $\mu_M = \tau_x/\sigma_y$. If the fracture process is generic, we would expect that $n_b(\sigma_y)$ behaves roughly similar to, e.g., acoustic emission counts observed during the compression of granular material [21]. This would correspond to our experiments in the limit $\tau_x \to 0$. As pressure is increased on a fragment-filled shear zone, the initial dilatancy due to cracking is again reduced by grinding. First, the most vulnerable grains break, and the new fragments move to fill up local pore space. As a pore space is filled up, a region will become much harder to break, and it will thereafter deform, mainly by elastic compression. As a larger fraction of local pore space is filled up, an ever increasing force is needed to squeeze grain fragments into the vanishing pore spaces. The exact relation between pressure and fracture is likely to be rather complicated and vary between different materials and environments. It may, nevertheless, be useful to postulate the simplest possible relation. This would be linear: $d\sigma_y/dn_b \propto \sigma_y$, resulting in an exponential function, $\sigma_y(n_b)$, or inversely, a logarithmic function $n_b(\sigma_y)$. Such behavior has been observed, e.g., by measuring acoustic emission counts during the compressive compaction of granules [22].

It is reasonable to set the unit of σ_y such that $\sigma_y = 1$ at the uniaxial compression strength (UCS) of a material. (I.e., σ_y is defined as the dimensionless pressure P/P_{UCS}, where P_{UCS} is the pressure at UCS.) When pressure is increased above UCS, the material will begin to disintegrate, and we would expect a transition to a more rapid increase in n_b: $d\sigma_y/dn_b \propto \mathrm{const}$. This UCS point typically marks the beginning of the transition zone from a brittle solid with a well-defined kinetic friction to the ductile and rate dependent friction of a powder, for which measured effective friction often decrease as strain rate is reduced [23,24].

The first spanning crack in the emerging shear zone typically has a very pronounced roughness. In order for shear motion to be possible without any fracture of the fragile crack surfaces, opposite sides of the shear zone

would have to rise over the roughness asperities, which implies significant dilation; i.e., σ_y must be low for dilation to occur rather than fracturing. As shear motion is forced under higher pressure, asperities and fragments begin to break, beginning at the locations that resist shear motion the most, and which therefore have the highest shear stress concentration. As these shear frustrations are broken, the grinding would continue with less significant shear pinning points. If, as above, we postulate a linear relation, we get $d\mu_M/dn_b \propto \mu_M$.

The above can be summarized as:

$$\begin{aligned} n_b &= c_1 \ln \sigma_y + c_2, \qquad \sigma_y < \sim 1, \\ n_b &= \bar{c}_1 \sigma_y + \bar{c}_2, \qquad \sigma_y > \sim 1, \end{aligned} \tag{1}$$

and

$$\mu_M = c_3 e^{n_b/c_4}, \tag{2}$$

where $\bar{c}_i$ and c_i, $(i = 1\text{–}4)$, are constants. These constants are not arbitrary: in the limit $n_b \to 0$, we have $\mu_M = c_3$. This would represent the very early phase when the shear zone is only a rough crack. We thus expect, $c_3 \sim 1.0$. Furthermore, if n_b is measured as the fraction of broken beams in our numerical model material, or the fraction of grain contact separation in granite, we expect $c_2 \sim 1$, as $c_2 = n_b$ at the brittle-ductile transition, at which point the material is already largely ground to a powder. There are not many general limitations on the constant c_4. If it is negative, friction will be reduced by a fracture, otherwise it is the opposite. If its absolute value is large, changes will be small, if not, changes in friction will be large with a fracture. Finally, we expect $\exp(-c_2/c_1)$ to be very small because $n_b = 0$ only for very small σ_y.

In order to test the above, we investigated numerically different types of brittle material models. Based on the results below, these materials can be divided into three different categories. (i) A material of spherical particles where the smallest possible fragments are single discs with a friction μ_m. Microscopic shear relaxation in this material is dominated by sliding for very small μ_m, and by fragment-on-fragment rolling for large μ_m. (ii) A material of "angular" particles and small μ_m. This material can be fragmented only so far that any disc remains connected to at least one other. With a small μ_m, shear stress can still be relaxed fairly easily by sliding. (iii) The third category is angular in the same way, but with a large μ_m. For this material there is no longer a mechanism to relax shear stress at the microscopic scale. In this case, μ_M is, more or less, independent of n_b until the beginning of the brittle-ductile transition regime is reached. I.e., as long as $\sigma_y < 1$. This would imply a larger absolute value for c_4 compared to the other two cases, for which we would expect that $c_4 \sim -10^{-1}$. In essence, these models together capture three significant deformation mechanisms for shear zones formed below UCS: fracture, rotation, and sliding [25]. To extend the numerical model to and above UCS, creep, plasticity, and viscoelasticity would need to be incorporated.

The values of the theoretical constants can be estimated based on numerical results. Best fits of such an exercise were: $c_3 \approx 1.02, 2.03, 1.56$, for (i) to (iii), respectively, which is consistent with the theoretical $c_3 \sim 1.0$. Best fits for the second constant were $c_2 \approx 0.424, 0.528, 1.515$, which is also consistent with its theoretical estimate $c_2 \sim 1$, even though the last value is obviously too large to be the fraction of broken beams, which means $n_b \sim 1$ in case (iii) already prior to UCS. We expect $c_4 \sim -10^{-1}$, except for (iii) in which case we expect a larger absolute value. Best fits gave: $c_4 \approx -0.251, -0.318, -4.686$. Finally, according to theory, c_1 should be significantly smaller than c_2. Best fits gave: $c_1 \approx 0.037, 0.045, 0.157$, respectively. Numerical results are shown in Fig. 2.

Above, μ_M is a function of σ_y and n_b, but macroscopic friction, μ_M, should also depend on microscopic friction μ_m. The effect of μ_m on $\mu_M(\sigma_y)$ can be reasonably well accounted for by the rescaling of parameters: $\mu_M \to \mu_M \mu_m^{\beta}$, and $n_b \to n_b \mu_m^{\alpha}$.

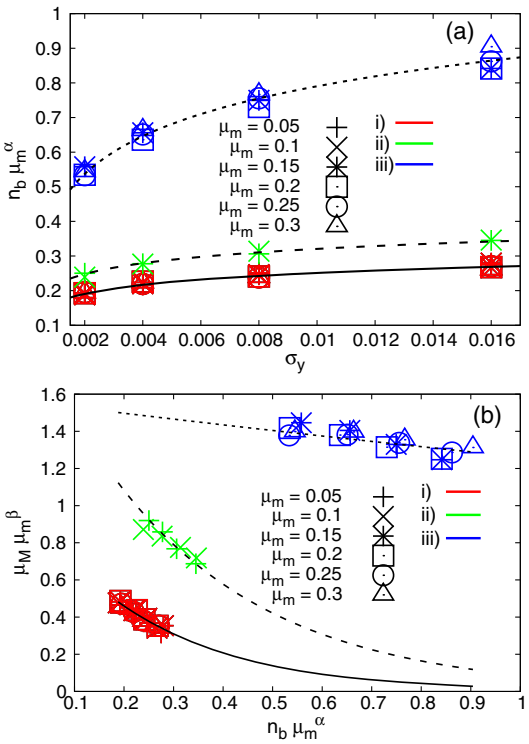

FIG. 2. Fraction of broken beams as a function of normal pressure (a) and macroscopic friction coefficient as a function of fraction of broken beams (b). The data has been rescaled with the parameters presented in the main text and fitted with Eqs. (3) and (5) in (a) and (b), respectively.

Equations (1) and (2) can then be written as:

$$n_b\mu_m^\alpha = c_1 \ln \sigma_y + c_2, \qquad \sigma_y < \sim 1, \tag{3}$$

$$n_b\mu_m^\alpha = \bar{c}_1\sigma_y + \bar{c}_2, \qquad \sigma_y > \sim 1, \tag{4}$$

$$\mu_M\mu_m^\beta = c_3 e^{n_b\mu_m^\alpha/c_4}. \tag{5}$$

By substituting Eq. (5) with Eqs. (3) and (4), we get

$$\mu_M\mu_m^\beta = c_3 e^{c_2/c_4}\sigma_y^{c_1/c_4}, \qquad \sigma_y < \sim 1,$$

$$\mu_M\mu_m^\beta = c_3 e^{\bar{c}_2/c_4} e^{\sigma_y \bar{c}_1/c_4}, \qquad \sigma_y > \sim 1. \tag{6}$$

In the cross-over region between brittle and emerging ductility, μ_M should be described by a smooth function, which sets constraints on the constants. We can then arrive at an approximate single function for $\mu_M(\sigma_y)$:

$$\mu_M = \mu_m^{-\beta} c_3 e^{c_2/c_4}\sigma_y^{c_1/c_4} \exp(-\sigma_y/c_5), \tag{7}$$

where $c_5 \sim 1$. The parameters for the three materials can be summarized as (i) $c_3 e^{c_2/c_4} \approx 0.19$, $\beta \approx -0.055$, $c_1/c_4 \approx -0.15$ (ii) $c_3 e^{c_2/c_4} \approx 0.39$, $\beta \approx -0.25$, $c_1/c_4 \approx -0.14$ (iii) $c_3 e^{c_2/c_4} \approx 1.13$, $\beta \approx -0.5$, and $c_1/c_4 \approx -0.034$.

For material (i), β is almost zero, which means that macroscopic friction has hardly any dependence on the friction of the fragments, μ_m. The reason for this is revealed in Tables I and II. Table I shows the ratio of average slip over average rotation for spherical particles. Only for large σ_y and $\mu_m = 0$ does sliding of fragments dominate over rotation as stress relaxation mechanism. For larger μ_m, rotations dominate completely. This means that there are mechanisms for relaxing microscopic, i.e., fragments scale, shear stress for all μ_m. This leads to a small $c_3 e^{c_2/c_4}$, and a nonzero c_1/c_4 resulting in a very low effective shear zone friction, μ_M, as pressure, σ_y, is increased. For material (ii), microscopic shear stress can still be efficiently relaxed by rotation as long as σ_y is very small, but for large σ_y, sliding always dominates. This means that shear stress can be relaxed only for small μ_m, i.e., material (ii). In this case, the absolute value of β is considerably increased, but c_1/c_4 is still nonzero, which means that μ_M decreases with increasing σ_y. Finally, for material (iii), fracture can no longer induce relaxation of microscopic shear stress, and fragments have to slide, even though μ_m is high. This leads to $c_1/c_4 \sim 0$. I.e., this material is not self-lubricating.

TABLE I. Total slip displacement divided by total angular rotation of the discs during a simulation with spherical particles. Italic entries slip/rot < 0.4, and bold entries slip/rot > 1.0.

	μ_m						
σ_y	0.0	0.05	0.1	0.15	0.2	0.25	0.3
0.002	0.494	*0.109*	*0.089*	*0.087*	*0.071*	*0.063*	*0.058*
0.004	0.822	*0.244*	*0.228*	*0.185*	*0.164*	*0.133*	*0.116*
0.008	**1.557**	0.497	*0.399*	*0.348*	*0.304*	*0.248*	*0.210*
0.016	**3.057**	0.725	0.635	0.548	0.463	*0.397*	*0.372*

TABLE II. Total slip displacement divided by total angular rotation of the discs during a simulation with angular particles. Italic entries slip/rot < 0.4, and bold entries slip/rot > 1.0.

	μ_m						
σ_y	0.0	0.05	0.1	0.15	0.2	0.25	0.3
0.002	*0.244*	*0.268*	*0.268*	*0.293*	*0.321*	*0.297*	*0.347*
0.004	0.512	0.515	0.480	0.617	0.646	0.746	0.779
0.008	0.870	0.921	**1.057**	**1.197**	**1.244**	**1.281**	**1.344**
0.016	**1.366**	**1.543**	**1.787**	**1.912**	**2.000**	**2.168**	**2.078**

In order to compare Eq. (7) to the data, we need to know μ_m and UCS. For the simulations these are easily determined. For the experiments on granite, we used $\mu_m = 0.5$ [26,27] and UCS = 119 MPa [28].

In order to further test the theory, check its scale invariance, and its relevance for tectonic faults, we tested how well Eq. (7) fits with what is observed at the San Andreas Fault Observatory at Depth (SAFOD). SAFOD reports that the fault gouge found in a creeping part of the fault contains quartz, corrensite, saponite, feldspar, and calcite [29]. The UCS values for these rock types have a relatively large range. The weakest is saponite, which has a UCS $\sim$ 10 MPa [30], while for, e.g., granular quartzite, the UCS = 200–500 MPa [31]. The exact value of the UCS for a composite material depends in a nontrivial way on its structure, and the exact value is not know to us. We therefore simply make the crude estimate that a reasonable value is UCS = 100 MPa, which is close to the estimated pressure inside the fault, 122 MPa [29]. For microscopic friction, we used $\mu_m = 0.2$ [26,32]. SAFOD data were extracted from references [21,33], and they are marked as SAFOD 1 and SAFOD 2 in Fig. 3, respectively.

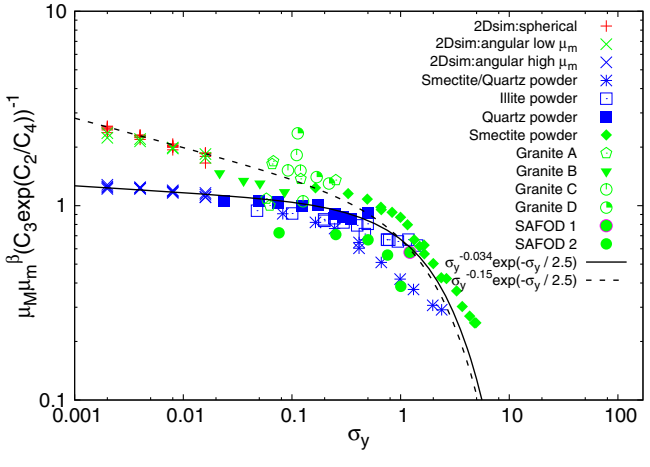

FIG. 3. Friction parameter $\mu_M\mu_m^\beta/(c_3 e^{c_2/c_4})$ as function of pressure σ_y for the three material classes (i) (red), (ii) (green), (iii) (blue). The data is compared to theoretical functions.

In addition, we compared the theory to friction experiments conducted on smectite, illite, and quartz powders under high relative pressures reported in Ref. [34]. For these data, we used the parameters: UCS = 30, 100, 200 MPa, and $\mu_m = 0.2$, 0.34, 0.35, respectively. The results are shown in Fig. 3. It is interesting to note that for these powders, the exponent c_1/c_4 is typically very small, which is consistent with the fact that powders are highly fragmented to begin with. One would then expect little or no increase in n_b with increasing σ_y below the UCS. This means $c_1 \sim 0$, consistent with the result.

In conclusion, we have demonstrated that there is self-lubrication by fragmentation within shear-fracture zones if there is a mechanism for stress relaxation at the microscopic scale of single grains or fragments. In the numerical model used here, this mechanism is either low-friction sliding or rotation. If neither of these mechanisms are present, no self-lubrication is observed in the investigated model. In the generic case, it is possible to imagine additional stress relaxation mechanisms that only need to appear locally at significant stress carrying contacts between fragments. Such mechanisms could be: partial melting, plastic deformations, creep, vibrations, ductile deformations, etc. In particular, for clay's frictional weakness, it is associated with interactions between the pore fluid and the chemically-charged clay surfaces [35]. In all cases, the arguments leading to Eq. (7) are still valid. Near and above the UCS, macroscopic friction decays fast and should become rate dependent. Here, we have been able to demonstrate the cross-over to a fast decay of μ_M, but not the exact dependence on rate. It should also be noted that our investigation only considers a constant confining pressure. A variable or cyclic loading may modify the friction behavior.

[1] G. Grasselli and P. Egger, Constitutive law for the shear strength of rock joints based on three-dimensional surface parameters, Int. J. Rock Mech. Min. Sci. Geomech. Abstr. **40**, 25 (2003).

[2] T. H. Huang, C. S. Chang, and C. Y. Chao, Experimental and mathematical modeling for fracture of rock joint with regular asperities, Eng. Fract. Mech. **69**, 1977 (2002).

[3] H. S. Lee, Y. J. Park, T. F. Cho, and K. H. You, Influence of asperity degradation on the mechanical behavior of rough rock joints under cyclic shear loading, Int. J. Rock Mech. Min. Sci. Geomech. Abstr. **38**, 967 (2001).

[4] M. S. Asadi and V. Rasouli, Direct shear test simulation of real rough rock fractures, *Rock Mechanics in Civil and Environmental Engineering*, edited by J. Zhao, V. Labiouse, J.-P. Dudt, and J.-F. Mathier (Taylor & Francis Group, London, 2010).

[5] A. Karami and D. Stead, Asperity degradation and damage in the direct shear test: A hybrid FEM/DEM approach, Rock mechanics and rock engineering **41**, 229 (2008).

[6] C. Lambert and C. Coll, Discrete modeling of rock joints with a smooth-joint contact model, JRMGE **6**, 1 (2014).

[7] K. Mair and S. Abe, 3D numerical simulations of fault gouge evolution during shear: Grain size reduction and strain localization, Earth Planet. Sci. Lett. **274**, 72 (2008).

[8] J. Park and J. Song, Numerical simulation of a direct shear test on a rock joint using a bonded-particle model, Int. J. Rock Mech. Min. Sci. Geomech. Abstr. **46**, 1315 (2009).

[9] Z. Reches and D. A. Lockner, Nucleation and growth of faults in brittle rocks, J. Geophys. Res. **99**, 18159 (1994).

[10] C. H. Scholz, Wear and gouge formation in brittle faulting, Geology **15**, 493 (1987).

[11] C. G. Sammis and S. J. Steacy, The micromechanics of friction in a granular layer, Pure Appl. Geophys. **142**, 777 (1994).

[12] J. De Bakker, Energy use of fine grinding in mineral processing, Metall. Mater. Trans. E **1**, 8 (2014).

[13] J. Jeswiet and A. Szekeres, Energy Consumption in Mining Comminution, Proc. CIRP **48**, 140 (2016).

[14] B. M. Carpenter, D. M. Saffer, and C. Marone, Frictional properties of the active San Andreas Fault at SAFOD: Implications for fault strength and slip behavior, J. Geophys. Res. **120**, 5273 (2015).

[15] J. R. Rice, Chapter 20 Fault Stress States, Pore Pressure Distributions, and the Weakness of the San Andreas Fault, Int. Geophys. **51**, 475 (1992).

[16] N. Kato and T. Hirono, Heterogeneity in friction strength of an active fault by incorporation of fragments of the surrounding host rock, Earth, Planets Space **68**, 134 (2016).

[17] J. R. Rice, Heating and weakening of faults during earthquake slip, J. Geophys. Res. **111**, n/a (2006).

[18] R. C. Viesca and D. I. Garagash, Ubiquitous weakening of faults due to thermal pressurization, Nat. Geosci. **8**, 875 (2015).

[19] T. I. Riikilä, T. Tallinen, J. Åström, and J. Timonen, A discrete-element model for viscoelastic deformation and fracture of glacial ice, Comput. Phys. Commun. **195**, 14 (2015).

[20] J. Åström, T. I. Riikilä, T. Zwinger, D. Benn, J. C. Moore, and J. Timonen, A particle based simulation model for glacier dynamics, Cryosphere **7**, 1591 (2013).

[21] D. Lockner, The role of acoustic emission in the study of rock fracture, Int. J. Rock Mech. Min. Sci. Geomech. Abstr. **30**, 883 (1993).

[22] L. Hégron, P. Sornay, and N. Favretto-Cristini, Compaction of a Bed of Fragmentable UO_2 Particles and Associated Acoustic Emission, IEEE Trans. Nucl. Sci. **61**, 2175 (2014).

[23] C. E. Renshaw and E. M. Schulson, Universal behavior in compressive failure of brittle materials, Nature (London) **412**, 897 (2001).

[24] J. C. Santamarina and H. Shin, *Friction in Granular Media, Meso-Scale Shear Physics in Earthquake and Landslide Mechanics* (CRC Press, Boca Raton, 2009) pp. 159–190.

[25] J. T. Engelder, Cataclasis and the Generation of Fault Gouge, Geol. Soc. Am. Bull. **85**, 1515 (1974).

[26] W. Derski, R. Izbicki, I. Kisiel, and Z. Mróz, *Rock and Soil Mechanics* (Polish Scientific Publishers, Warsaw, 1989).

[27] S. Mandal and R. Maiti, *Semi-quantitative Approaches for Landslide Assessment and Prediction* (Springer, Singapore, 2015).

[28] P. Eloranta, Laboratory Testing of Gneissic Rocks in Olkiluoto Borehole Ol-KR24, Posiva, working report 2006-80, 2006.

[29] D. A. Lockner, C. Morrow, D. Moore, and S. Hickman, Low strength of deep San Andreas fault gouge from SAFOD core, Nature (London) **472**, 82 (2011).

[30] Petrowiki, http://petrowiki.org/Compressive_strength_of_rocks (2016).

[31] R. Pusch, *Geological Storage of Highly Radioactive Waste* (Springer, Berlin, 2008).

[32] H. M. Horn and D. U. Deere, Frictional characteristics of Minerals, Geotechnique **12**, 319 (1962).

[33] B. M. Carpenter, D. M. Saffer, and C. Marone, Frictional properties and sliding stability of the San Andreas fault from deep drill core, Geology **40**, 759 (2012).

[34] D. M. Saffer and C. Marone, Comparison of smectite- and illite-rich gouge frictional porperties: application to the undip limit of the seismogenic zone along subduction megathrusts, Earth Planet. Sci. Lett. **215**, 219 (2003).

[35] Diane E. Moore and David A. Lockner, *Friction of the Smectite Clay Montmorillonite, The Seismogenic Zone of Subduction Thrust Faults*, edited by T. H. Dixon and J. C. Moore, (Columbia University Press, New York, 2007) pp. 317–345.